Processing, Microstructure and Properties of Ti-6246

C.SAUER, G.LÜTJERING

Technical University Hamburg – Harburg, 21071 Hamburg, Germany

ANNOTATION
Different microstructures were generated in Ti-6Al-2Sn-4Zr-6Mo by different processing routes and the resulting properties were evaluated. The generated microstructures were of the β-annealed, α+β recrystallized and through β transus processed type. Tensile tests, S-N curves and K_{IC} tests were measured at room temperature for all microstructures. The paper will discuss the results in terms of microstructure / property relationships.

Key words: Ti-6246, α+β titanium alloys, β titanium alloys, processing, mechanical properties

1. INTRODUCTION

The alloy Ti–6246 (Ti-6Al-2Sn-4Zr-6Mo), developed by TIMET, is a high strength alloy for intermediate temperature applications up to about 300°C, particularly in discs and fan blades in the compressor part of gas turbine engines. It combines the long-time elevated temperature strength of Ti-6Al-2Sn-4Zr-2Mo, with the high short-term strength of a fully hardened α+β titanium alloy [1], [2]. The high room temperature strength results from high solid solution strengthening and from the good heat treatment response, which is due to the beta stabilizing effect of the six percent molybdenum.
The alloy exhibits full strength hardenability even in thick sections, sufficient ductility and toughness. However, the mechanical properties of Ti-6246 parts are even more sensitive to variations in processing parameters than those of α+β alloy type products. Therefore, it is important to investigate the influence of the thermomechanical treatment on microstructure, and further to obtain a fundamental understanding of the relation between microstructure and mechanical properties. In this paper, the processing routes to generate three different types of microstructures in Ti-6246, a β-annealed ("lamellar"), a α+β recrystallized ("bi-modal") and a through β transus processed ("necklace") microstructure, will be described, and the mechanical properties of these microstructures (tensile properties, HCF strength and fracture toughness) will be compared and evaluated.

2. MATERIAL AND EXPERIMENTAL PROCEDURE

The alloy Ti-6246 (Ti-5.8Al-2.0Sn-4.0Zr-6.1Mo-0.1O, wt.%, β-transus: 945°C) was produced by TIMET Metals Corp., UK. It was made available by Otto Fuchs Metallwerke, Germany, as round billets (ø:240 mm) in an α+β forged condition.

2.1. Thermomechanical Treatment

Deformation of the material was either performed by hot cross rolling (bi-modal microstructure, rolling degree ϕ=-1.2, initial block size 37 x 40 x 55 mm³) or hot unidirectional rolling (necklace microstructure, rolling degree ϕ=-1.0, initial block size 28 x 50 x 40 mm³), using a 700 kN duo mill. Heat treatments were performed in tube furnaces under inert gas atmosphere to prevent excessive oxidation.
The processing routes which were used to generate the different microstructures are schematically illustrated in Figures 1a-e.
A fully lamellar structure was generated by heat treatment alone (Figure 1a). After annealing in the single phase β field at 970°C for 1 hour and controlled cooling (50°C/min), a two step aging treatment was applied, consisting

of high temperature aging (1h 910°C / 50°C/min) and low temperature aging (8h 595°C / AC). For comparability, this two step aging treatment was identical for all microstructures.
As β-annealing alone leads to a fairly large β grain size of about 400 μm (Figure 2a), a lamellar microstructure with a smaller β grain size was generated for comparison by modifying the heat treatment as presented in Figure 1b. The material was rolled in the α+β phase field (900°C, ϕ=-1.0) and annealed slightly above the β-transus at 950°C for 1 hour. After cooling from the β phase field at a cooling rate of 50°C/min, the final aging treatment described above, was applied.
For the bi-modal microstructure, the as-received material was rolled in the α+β region at 905°C (followed by air cooling) and then annealed high in the α+β phase field at 935°C for 1 hour (cooling rate 50°C/min). This is illustrated in Figure 1c. The subsequent two step aging treatment was identical to the other microstructures.
In order to obtain a necklace type of microstructure, the as-received material was annealed in the β phase field at 970°C for 1 hour and then rolled through the β transus down to the α+β region (Figures 1d,e). During the procedure shown in Figure 1d, the material was put back into the rolling furnace after each deformation step for about 30 seconds. That was not long enough to compensate for the loss of heat of the plate being in contact with the cold rolls. So the deformation temperature decreased rapidly to about 800°C. After the rolling was completed, the plate was furnace-cooled with an initial rate of approximately 7°C/min. A modification of this rolling procedure is shown in Figure 1e. In this process, again the deformation was started in the β phase field, but after passing through the transus, the rolling was continued isothermally at a temperature of 935°C. After the last rolling step, the plate was air cooled.
Both deformation procedures were followed by the two step aging treatment as described.

2.2. Microscopy and Mechanical Tests

The obtained microstructures were investigated by light microscopy (LM) and transmission electron microscopy (TEM). The LM samples were mechanically polished and etched either in Kroll's reagent or glycerol + HF (50:1). The TEM foils were electrolytically thinned and investigated in a Philips 400ST microscope at 120 kV. Fracture surfaces of the S-N specimens were investigated in the SEM (Jeol 840, 20kV).
Tensile tests were performed using a 50 kN spindle driven testing machine at an initial strain rate of $8 \cdot 10^{-4} s^{-1}$.
S-N curves were measured in rotary bending mode (R=-1, 50 Hz, air). The S-N specimens were hour-glass shaped (minimum diameter 3.8 mm) and electrolytically polished prior to testing in order to exclude any effect of the machined surface on the fatigue properties.
The fracture toughness tests were performed on single edge notched four-point bend specimens (thickness 8 mm). According to ASTM E399, the specimens were precracked in fatigue (R=0.2, 80 Hz, air) and afterwards bent to fracture at a loading rate of 0.1 mm/min. The crack front profiles of these specimens were investigated by taking sections perpendicular to the crack propagation direction. Those sections were studied in the light microscope.
For the necklace microstructure, the mechanical tests were performed with the stress axis perpendicular to the rolling direction (LT-direction). The crack propagation in the fracture toughness tests was in L-direction.

3. RESULTS AND DISCUSSION

3.1. Microstructures

Figures 2a, b (LM) and Figure 2c (TEM) show the lamellar microstructure resulting from the heat treatment presented in Figure 1a. The β annealing resulted in large equiaxed β grains with a grain size of about 400 μm (Figure 2a). Upon cooling, continuous grain boundary α layers and α plates within the β grains developed. The subsequent high temperature aging coarsened the α plates. During low temperature aging, a high volume fraction of fine secondary α platelets was precipitated (Figure 2c). The microstructure contains a high volume fraction of coarse α plate colonies in the neighborhood of the β grain boundaries (Figure 2a,b). Within these colonies, the coarse α plates are crystallographically parallel. In the center area of the grains, the coarse α plates have a Widmanstaetten type of morphology (Figure 2a,b).
The modified process (Figure 1b) led to a smaller average β grain size of about 200 μm as shown in Figure 2d. Rolling in the α+β phase field produced a high dislocation density, and consequently a high density of nucleation sites for new β grains was present during recrystallization in the β field, leading to smaller β grains. Still, some large β grains were occasionally observed in the microstructure. Some individual grains may have been unfavorably oriented in relation to the stress direction during rolling, so that the degree of deformation introduced in these regions was not sufficient to trigger fine recrystallization. This could be improved by

applying a multiaxial deformation. Grain boundary α layers and α plate colonies are observed also in this microstructure.
The bi-modal microstructure is presented in Figures 3 a (LM) and 3b (TEM). During the α+β annealing at 935°C following the deformation, both α and β phases recrystallized. The recrystallization was performed close to the β transus, resulting in a rather low volume fraction of globular primary α grains (about 15%, average diameter 4 μm). The globular primary α grains "pin" the β grain boundaries, leading to a fairly small β grain size of about 20 μm (Figure 3a). The high temperature aging caused the precipitation of coarse α plates (Figure 3a), low temperature aging formed a high volume fraction of fine secondary α platelets (Figure 3b).
Figures 4a,b (LM) and Figure 4c (TEM) show the necklace microstructure obtained by the process illustrated in Figure 1d. The through transus rolling after homogenization resulted in a pancake shaped β grain structure (Figure 4a) with chains of discontinuous α particles along the β grains. Because a major part of the deformation was performed at rather low temperatures in the α+β field (as low as 800°C), a high density of dislocations was generated. Dislocations act as nucleation sites for α particles, and their high density led to a fine precipitation of α plates in the β grains. The modified rolling procedure (Figure 1e) resulted in the same β grain size and shape (Figure 4d), but the α plates within the grains were coarser. This is due to the fact that the formation of α occurred in a much more recovered microstructure, because a major part of the rolling was performed isothermally at a comparatively high temperature. Also the α plates along the β grain boundaries were more elongated, compared to the more globular particles in the other ("fine") necklace structure. Again, high temperature aging was performed to coarsen the α plates in both necklace structures, and low temperature aging formed small α platelets.

3.2. Tensile Properties

The tensile properties for the different microstructures are shown in Table 1. All microstructures exhibited high yield stresses due to the close spacing of incoherent α particles. This effectively hinders dislocation movement, following the Orowan relationship. The bi-modal microstructure showed the highest yield stress (1105 MPa), which is probably due to an additional strengthening effect of the small β grain size. The lamellar microstructures exhibited a significantly lower yield stress (995 MPa). This is due to the high volume fraction of α plate colonies in the neighborhood of the β grain boundaries. Within these colonies, the α plates are crystallographically parallel, allowing easy slip transfer from one plate to the next, and therefore leading to a lower yield stress as the effective slip length is increased. The yield stress of the necklace structures was also very high (1100 MPa and 1085 MPa, respectively), which results from the comparatively small phase dimensions.
The coarse grained lamellar structure showed the lowest ductility (RA=5.6 %), which is due to premature failure along the soft continuous grain boundary α layers in conjunction with the large β grain size. By decreasing the grain size to 200 μm, the ductility could be increased to RA=17.1 %, as the effective length of the grain boundary α layers was significantly reduced. In the bi-modal Microstructure, the grain boundary α layers were very short because of the small β grain size, resulting in a high ductility (RA=37.7 %). The necklace microstructures (tested in LT-direction) also exhibited good ductility, as continuous α layers were absent. It has to be emphasized that, due to the strongly textured β grains, the properties of the necklace type of microstructures are highly anisotropic. In the present work, the short transverse (ST) direction was not tested, but Peters [3] found , studying β-Cez, lower ductility and drastically lower fracture toughness in the ST-direction as compared with L - or LT-direction.

3.3. Fracture Toughness

The measured fracture toughness values are presented in Table 1. There are several microstructural parameters influencing fracture toughness [4]. Assuming identical fracture mechanisms in the tensile test and the fracture toughness test, one of those parameters is tensile ductility, because it represents the intrinsic fracture properties of the material in a first approximation. Ductility itself is influenced by the effective β grain size, but also by β grain shape. As already discussed, the bi-modal microstructure and the necklace microstructures (tested in LT-direction) exhibited good ductility, while the ductility of the lamellar structure was low.
Another major parameter affecting fracture toughness is the crack front geometry, because a rough crack front effectively hinders crack advance. The crack front profiles of the bi-modal, the lamellar (400μm) and the necklace (fine α plates) microstructure is shown in Figures 5a-c. The crack tends to propagate along the β grain boundaries if possible, due to the large plastic zone at the crack tip. The crack front geometry is determined by the β grain size and shape. The small β grain size of the bi-modal microstructure resulted in a very flat crack front profile (Figure 5b), because the crack is not much deflected propagating along the β grain boundaries.

Compared to that, the large equiaxed β grains of the lamellar microstructure caused a very serrated and rugged crack front (Figure 5a). The crack front profile of the necklace microstructure is strongly depending on the orientation of the pancake-shaped β grains relative to the stress axis. Upon testing in L- or LT-direction, one long axis of the pancake grains is parallel to the stress direction. Although unfavorably oriented, the crack advances partially along the necklace chains of discontinuous α, which results in a rough crack front (Figure 5c). Partially, the crack advances through the matrix. Then the α plate dimensions have to be taken into account as another parameter influencing fracture toughness, because large α plates result in a higher crack deflection than small plates. It can be seen in Figures 2-4, that the lamellar structures show the largest α plates, followed by the bi-modal microstructure, while the α plates in the necklace microstructure are comparatively fine.
The measured fracture toughness values result from a superimposition of the described effects. The low fracture toughness of the bi-modal microstructure (K_Q=43 MPa m $^{1/2}$) as compared to the lamellar (K_Q=58 MPa m $^{1/2}$) and necklace (K_Q=62 MPa m $^{1/2}$) microstructures shows, that the crack front geometry is the dominating effect, while ductility and α plates are less influential. The flat crack front of the bi-modal structure outweighs the positive influence of the high ductility and the fairly large α plates, resulting in a comparatively low fracture toughness. The rough crack front of the lamellar structure overcompensates the negative influence of the low ductility, resulting in a high fracture toughness. The high fracture toughness of the necklace microstructures is also due to the rough crack front, and the good ductility may have an additional positive effect. The negative effect of relatively small α plates is subordinate. Again, it has to be mentioned, that the fracture toughness properties of the necklace microstructures are highly anisotropic. Testing in ST-direction would most probably result in low fracture toughness [3].

3.4. Fatigue Properties

The measured S-N curves are shown in Figure 6. SEM pictures of the fracture surfaces of some fatigue specimens are presented in Figures 7a-c. It can be seen from Figure 6, that the necklace microstructure exhibited the highest HCF (high cycle fatigue) strength ($\sigma_{10}7$= 600 MPa), followed by the bi-modal structure ($\sigma_{10}7$= 575 MPa). The lowest HCF strength was measured for the lamellar structures ($\sigma_{10}7$= 525 MPa). In the HCF regime, fatigue strength is dominated by the resistance against crack nucleation. For crack nucleation, dislocation movement is necessary. So, the HCF strength is often correlated to the yield stress [5]. This is one possible explanation for the low HCF strength of the lamellar structure, as it showed a significantly lower yield stress than the other microstructures. Besides that, a direct influence of the microstructural morphology on the fatigue crack nucleation resistance is observed. Figure 7a shows the fracture surface of a lamellar fatigue specimen. It can be seen, that the fatigue crack has nucleated at the α/β interface of the soft continuous α layer along a β grain boundary. The presence of the continuous α layer resulted in a low resistance against fatigue crack nucleation, and therefore in a low HCF strength. The highest HCF strength was measured for the necklace microstructures. Figure 7c shows the fracture surface of a fatigue specimen of the necklace structure (fine α plates). The figure indicates that the fatigue crack has nucleated at the necklace chain of discontinuous α along the β grain boundaries. A continuous α layer was absent in this microstructure, and as the α particles along the β grain boundaries are rather small, the stress concentration in the α/β interfaces was low, resulting in a higher fatigue crack nucleation resistance, even compared with the bi-modal microstructure. For the bi-modal microstructure, the crack nucleation site could not be determined exactly. The fracture surface of one specimen is shown in Figure 7b. It can be assumed that the fatigue crack nucleated along an α/β interface. Because both, the globular primary α grains and the coarse α plates, which are present in the bi-modal structure, are larger than the grain boundary α particles in the necklace microstructures (compare Figure 3a with 4b and with 4d), this might serve as a possible explanation for the superior crack nucleation resistance of the necklace structures as compared to the bi-modal structure.

4. CONCLUSIONS

- Tensile, fracture toughness and HCF properties of the Ti-6246 alloy exhibited a strong influence of microstructure.
- The bi-modal microstructure exhibits high yield strength, but the fracture toughness was relatively low.
- The lamellar microstructure showed low ductility. Reducing the β grain size by deformation and recrystallization increased ductility.
- The necklace microstructure exhibited the best combination of properties, but the mechanical properties are anisotropic.

5. REFERENCES

1. R.R. BOYER, G.WELSCH, E.W.COLLINS (Ed.): "*Materials Properties Handbook: Titanium Alloys*", ASM International, Materials Park, Ohio, 1994, p.465-481.

2. TIMET TECHNICAL SERVICE DEPARTMENT: "*Metallurgical and Mechanical Properties of an Advanced High Strength Titanium Alloy Ti-6Al-2Sn-4Zr-6Mo*", TIMET Metals Corp.

3. J.O.PETERS, G.LÜTJERING: "Processing, Microstructure and Properties of β-Cez", *Titanium '95: Science and Technology*, 1996, **Vol. 2**, p.1403-1410.

4. G.LÜTJERING, A.GYSLER, L.WAGNER: "Crack Propagation in Ti-Alloys", *Proceedings Sixth World Conference on Titanium*, 1988, **Vol. 1**, p.71-p.80.

5. G.LÜTJERING, A.GYSLER: "Fatigue", Critical Review, *Titanium Science and Technology*, DGM, 1984, **Vol. 4**, p.2065-2083

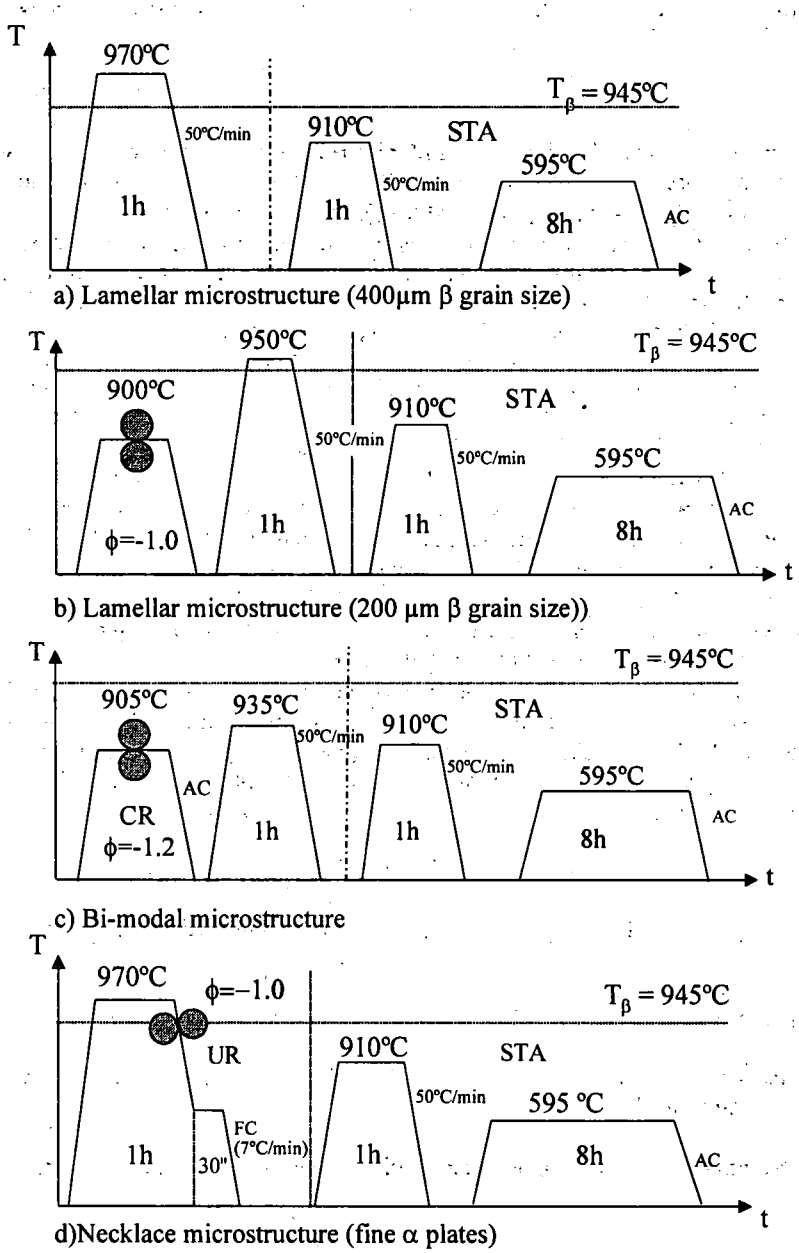

Fig.1: Schematic illustration of thermomechanical treatments

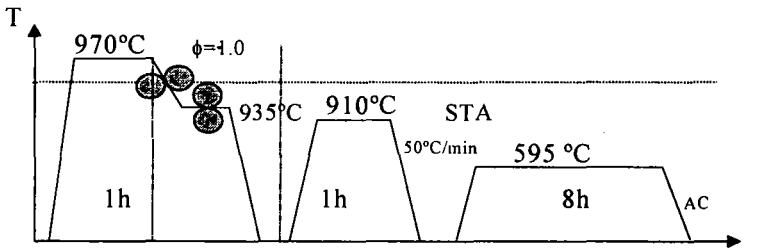

e) Necklace microstructure (coarse α plates)

Fig.1 (contd.): Schematic illustration of thermomechanical treatments

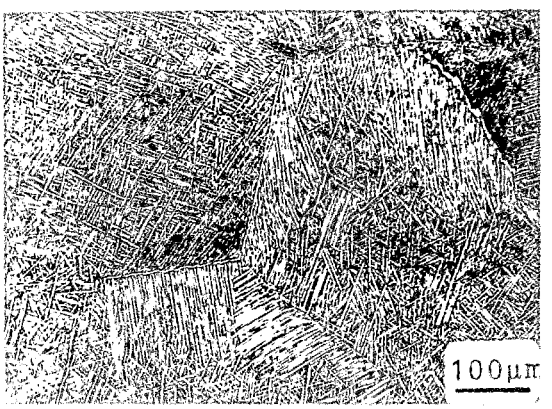

a) Lamellar 400μm, LM

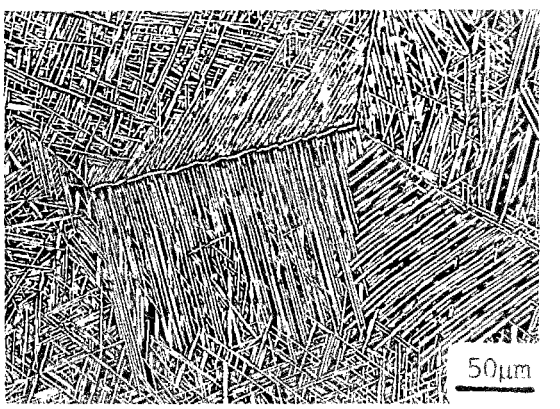

b) Lamellar 400μm, LM

c) Lamellar 400μm, TEM

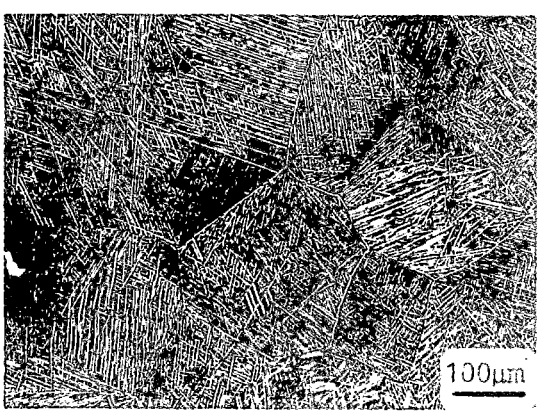

d) Lamellar 200μm, LM

Fig.2: Lamellar microstructures

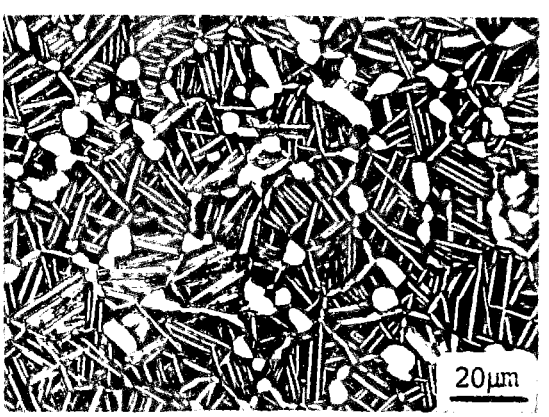

a) LM

b) TEM

Fig. 3.: Bi-modal microstructure

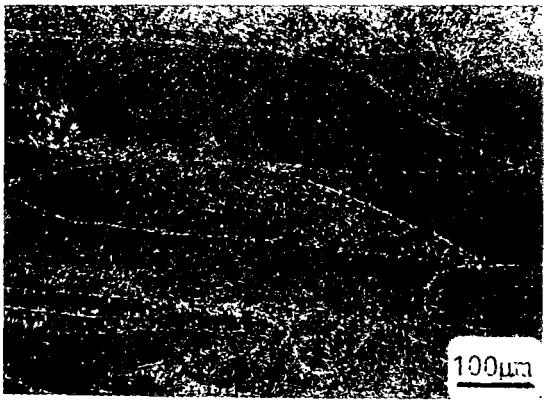

a) Necklace Fine, LM

b) Necklace Fine, LM

c) Necklace Fine, TEM

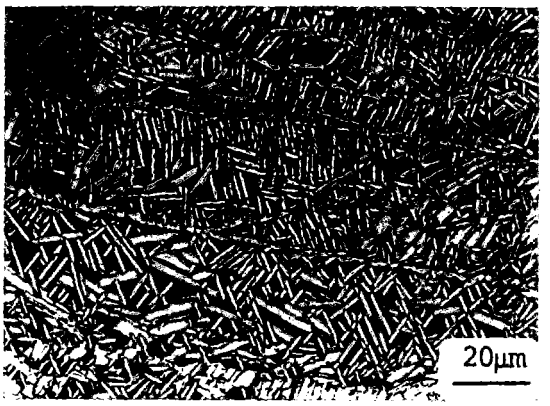

d) Necklace Coarse, LM

Fig. 4: Necklace microstructures

Table 1: Tensile Properties and HCF Properties

	E(GPa)	$\sigma_{0.2}$ (MPa)	UTS (MPa)	σ_f (MPa)	El.(%)	RA (%)	K_Q (MPam$^{1/2}$)
Bi-modal	118	1105	1200	1640	13.8	37.8	43
Lamellar 400µm	116	995	1115	1150	3.7	5.6	58
Lamellar 200µm	117	995	1105	1300	5.6	17.1	60
Necklace Fine (LT)	116	1085	1155	1445	11.0	20.1	59
Necklace Coarse (LT)	120	1100	1180	1450	11.4	24.3	62

a) Lamellar 400µm, K_Q=58 MPa m $^{1/2}$

b) Bi-modal, K_Q=43 MPa m $^{1/2}$

Fig. 5: Crack front profiles (LM), K_{IC}- test, 4-point-bending specimens

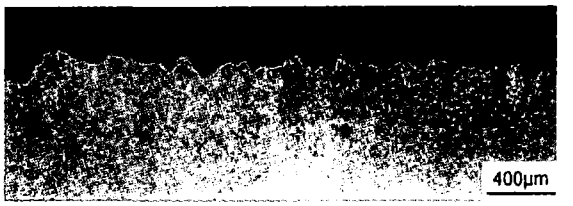

c) Necklace Coarse, K_Q=62 MPa m $^{1/2}$

Fig 5.(contd.): Crack front profiles (LM), K_{IC}- test, 4-point-bending specimens

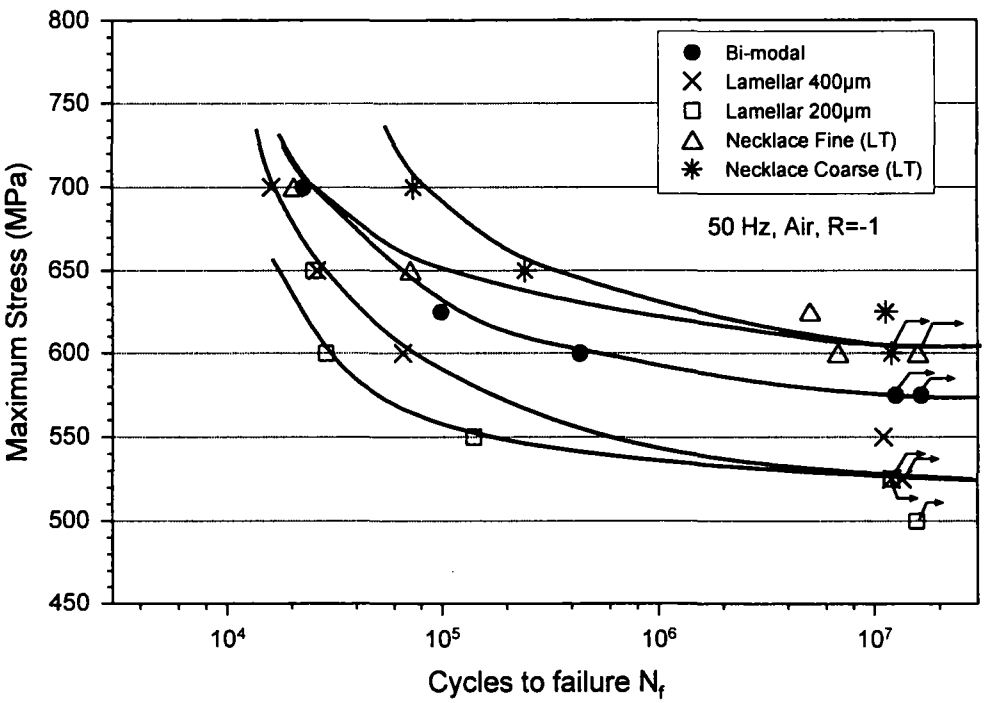

Fig. 6: S-N Curves, R=-1, air, 50 Hz

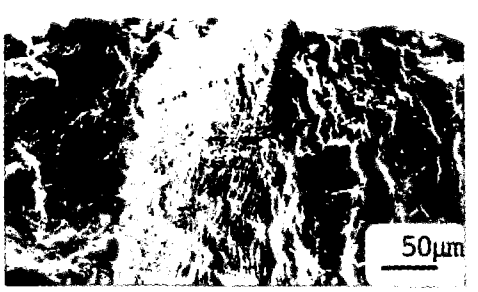

a) Lamellar 400µm, σ_{max}=650 MPa

b) Bi-modal, σ_{max}=625 MPa

c) Necklace Fine, σ_{max}=700 MPa

Fig. 7: Fracture surfaces S-N- specimens (SEM) , R=-1, air, 50 Hz